Simulation of Nanoparticle Agglomerate Fluidization Based on Continuum Theory of Cohesive Particles

Wu, Yan; Liu, Daoyin; van Wachem, Berend G.M.; van Ommen, J. Ruud

DOI
10.1021/acs.iecr.4c00310

Publication date
2024

Document Version
Final published version

Published in
Industrial and Engineering Chemistry Research

I&EC research
Industrial & Engineering Chemistry Research

pubs.acs.org/IECR

Article

Simulation of Nanoparticle Agglomerate Fluidization Based on Continuum Theory of Cohesive Particles

Yan Wu, Daoyin Liu,* Berend G. M. van Wachem, and J. Ruud van Ommen

Cite This: https://doi.org/10.1021/acs.iecr.4c00310

Read Online

ACCESS | Metrics & More | Article Recommendations | Supporting Information

ABSTRACT: Nanoparticles are usually fluidized as agglomerates, which are in dynamic states of agglomeration and fragmentation. It is critical to consider the size distribution of agglomerates in modeling of the fluidization of nanoparticle agglomerates. In this article, the fluidization behavior of nanoparticle agglomerates is investigated using a two-fluid model—population balance model. The model includes the agglomeration and breakage kernel functions based on the continuum theory of cohesive particles developed by Kellogg et al. (*J. Fluid Mech.* **2017**;832:345−382). The ratio of the critical breakage velocity to the critical agglomeration velocity is defined to represent the cohesion of nanoparticles. The predictions of bed pressure drop, bed expansion ratio, and bed collapse curves agree well with those of experiments. By changing the critical agglomeration velocity and the ratio between the critical velocities, the transition from almost defluidization to uniform fluidization is predicted. Finally, the model's ability to simulate the fluidization of fine particles with a few micrometers is also shown. This study provides a practical tool for simulating the fluidization of nanoparticle agglomerates.

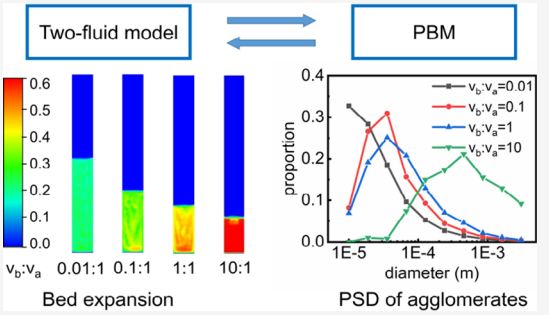

1. INTRODUCTION

Atomic layer deposition (ALD) is a thin film deposition technique based on ordered, self-saturated reactions, which can achieve a uniform coating on various functional materials on the subnanometer scale.[1,2] Fluidized bed reactors (FBRs) have high heat and mass transfer rates and are efficient facilities for processing particles. In recent years, the combination of FBR and ALD has become a promising coating technology for coating nanoparticles,[3,4] which is increasingly used in catalysts, electrode materials, and pharmaceutical materials.[5−7]

Nanoparticles refer to ultrafine particles with a particle diameter range of 1−100 nm, which show high cohesion[8,9] and are usually agglomerated.[10−12] In fluidized beds, agglomerates are dynamically formed, broken up, and present a wide size distribution.[13,14] Numerous experiments have shown that the size of fluidized agglomerates ranges from a few micrometers to a few hundred micrometers, with a highly porous structure.[15,16] Agglomerates have a multilevel fractal structure, whose irregular structure is usually quantified by a fractal dimension.[17,18] Due to the large specific surface area of nanoparticle agglomerates, there are differences in the transport rate of precursors between agglomerates and flat plates, which can affect the optimization of reaction parameters.[19] The dynamics of nanoparticle agglomerates and vapor deposition also interact with each other.[20] Therefore, studying the details of nanoparticle agglomerates inside a fluidized bed is very useful for optimizing and improving the efficiency of ALD reactions in the FBR.

Because nanoparticles show cohesion, it is indispensable to include a cohesion model for simulating the fluidization of nanoparticles. Besides, accurately describing the wide size distribution of agglomerates is crucial. In a broader view, there are mainly two kinds of simulation models for cohesive particle fluidization: the discrete element model (DEM) and the two-fluid model (TFM).

The DEM model tracks each agglomerate motion and examines the effect of interagglomeration cohesive forces on fluidization, by including a model that deals with the interactions between cohesive particles.[21−23] This method is based on Newton's second law to solve the motion of each particle and realize the individual tracking of particles.[24] In particular, particle cohesion can be considered directly by calculating the interparticle forces, such as the van der Waals force, liquid bridge force, and electrostatic force.[25] Li et al.[26] incorporated cohesive van der Waals forces into MFIX-DEM simulations, compared qualitative and quantitative information between numerical simulations and experimental measurements, and also investigated their influences on flow hydrodynamics. Wu et al.[27] studied the influence of cohesion on the discrete and continuum properties of particle fluidization by coupling the CFD-DEM approach and a weighted time-volume averaging method. The

Received: January 24, 2024
Revised: March 28, 2024
Accepted: March 29, 2024

results illustrate an important relationship between the microscopic and the macroscopic properties of the fluidization of cohesive particles. Bahramian et al.[28] numerically studied the impact of adhesion force and surface cohesiveness on the minimum fluidization velocity and PSD of nanoparticle agglomerates by applying a coupled CFD-DEM approach. However, the model is computationally intensive and cannot be directly applied to large-scale, or even laboratory-scale fluidized beds.[29]

The TFM model of hydrodynamics in fluidized beds of cohesive fine powders also attracts wide attention.[30−32] There are two main methods for considering agglomerate sizes in the frame of TFM. One method is the calculation of agglomerate size based on the balance between the cohesive forces and the separating forces.[33−35] However, this is an estimate of the final agglomerate size and does not allow for prediction of dynamic agglomeration and fragmentation, which results in difficulty in modeling the agglomerate size distribution. The other method uses the population balance model (PBM) to predict agglomerate dynamics during fluidization or gas−solid flows.[36,37] The PBM describes the variation in the number density of agglomerates within the system resulting from agglomeration and fragmentation, which can be used to calculate the agglomerate sizes dynamically during fluidization. In the studies by Kellogg et al.,[38,39] a continuum theory for lightly cohesive particles has been developed by taking into account both the population equilibrium of cohesive particles and the additional collisional dissipation and has been successfully applied to a lightly cohesive system with binary particle sizes. Recently, Bhoi et al.[40] developed a population balance framework for nanoagglomerates fluidization, which considered agglomeration and breakage phenomena and incorporated the fractal dimension property, and the influence of model parameters was investigated.

Through the above analysis, the combination of the TFM model and the PBM model is an efficient method for studying the macroscopic fluidization of nanoparticle agglomerates. However, due to the diversity of the structural properties of nanoparticle agglomerates and the complexity of collisions, further research is needed to develop more comprehensive agglomeration and breakage kernel functions.

In Kellogg et al.'s study,[38] the population equilibrium of cohesive particles is applied to lightly cohesive system with binary particle sizes. In this study, in order to simulate the fluidization more realistically, the continuum theory of Kellogg et al.[38] is combined with the general PBM model to describe a wider size distribution. First, the model is validated with different cases: an unbound riser system and extreme conditions (only agglomeration or only breakage) in a fluidized bed system. After that, the simulation of SiO_2 and TiO_2 particle fluidization is compared with experiments. Then, the effect of different critical velocities and their ratios on fluidization behaviors is investigated and explored. Finally, the model is also applied to a fluidized bed of fine particles with a few micrometers.

2. MATHEMATICAL MODEL

Figure 1 shows a schematic of the TFM-PBM model. The fluidization of nanoparticle agglomerates is modeled in a TFM framework with a PBM model by considering the effects of agglomeration and fragmentation between agglomerates. In the PBM equation, $\alpha(V, V')$ is the agglomeration rate of agglomerates with volumes of $V-V'$ and V'; p_0 is the number

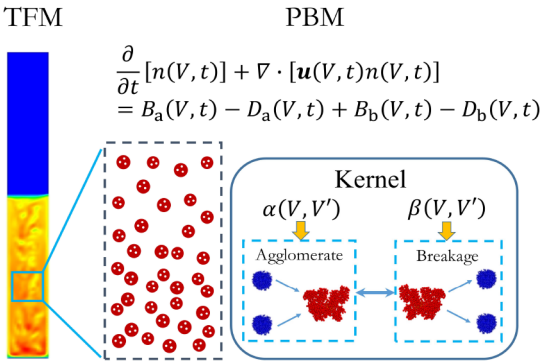

Figure 1. Schematic of the TFM-PBM model.

of parent agglomerates broken into subagglomerates; $\beta(V, V')$ is the probability of fragmentation of agglomerates with volume V.

2.1. Two-Fluid Model. The TFM model considers both the gas and nanoparticle agglomerates as continuums, both of which follow the continuity and momentum equations.[41−45]

2.1.1. Mass Conservation Equations.

$$\frac{\partial}{\partial t}(\varepsilon_g \rho_g) + \nabla \cdot (\varepsilon_g \rho_g \boldsymbol{u}_g) = 0 \tag{1}$$

$$\frac{\partial}{\partial t}(\varepsilon_s \rho_s) + \nabla \cdot (\varepsilon_s \rho_s \boldsymbol{u}_s) = 0 \tag{2}$$

$$\varepsilon_g + \varepsilon_s = 1 \tag{3}$$

where ε is the volume fraction, ρ is the density, and $\boldsymbol{u}$ is the velocity. The subscript g means gas, and subscript s means solid.

2.1.2. Momentum Conservation Equations.

$$\frac{\partial}{\partial t}(\varepsilon_g \rho_g \boldsymbol{u}_g) + \nabla \cdot (\varepsilon_g \rho_g \boldsymbol{u}_g \boldsymbol{u}_g) = -\varepsilon_g \nabla p + \nabla \cdot \varepsilon_g \tau_g + \varepsilon_g \rho_g g - \beta(\boldsymbol{u}_g - \boldsymbol{u}_s) \tag{4}$$

$$\frac{\partial}{\partial t}(\varepsilon_s \rho_s \boldsymbol{u}_s) + \nabla \cdot (\varepsilon_s \rho_s \boldsymbol{u}_s \boldsymbol{u}_s) = -\varepsilon_s \nabla p + \nabla \cdot \varepsilon_s \tau_s - \nabla p_s + \varepsilon_g \rho_g g + \beta(\boldsymbol{u}_g - \boldsymbol{u}_s) \tag{5}$$

where p is the pressure, τ is the viscous stress tensor, and β is the gas−solid drag coefficient.

2.1.3. Drag Model. The Gidaspow drag model[41] is adopted in this article. This model combines Ergun drag correlation and the Wen−Yu drag correlation.

The formulas of the Gidaspow drag model are as follows:

$$\beta_{gs} = \begin{cases} 150\dfrac{(1-\varepsilon_g)\varepsilon_s \mu_g}{\varepsilon_s d_2^{a}} + 1.75\dfrac{\rho_s \varepsilon_s |\boldsymbol{u}_g - \boldsymbol{u}_s|}{d_a} & (\varepsilon_s > 0.2) \\ \dfrac{3}{4} C_d \dfrac{|\boldsymbol{u}_g - \boldsymbol{u}_s|}{d_a} \varepsilon_g^{-2.65} & (\varepsilon_s \le 0.2) \end{cases} \tag{6}$$

where μ_g is the gas viscosity, d_a is the particle diameter, C_d is the drag coefficient, and Re is the Reynolds number of solid phase: $Re_s = d_a \varepsilon_g \rho_g |u_g - u_s| / \mu_g$.

2.1.4. Solid-Phase Closures. Fluctuation energy conservation of solid particles is solved by modeling the granular temperature (T_s), which is explained well in the literature.[44] The constitutive equations, e.g., granular viscosity, solid pressure, and frictional

https://doi.org/10.1021/acs.iecr.4c00310
Ind. Eng. Chem. Res. XXXX, XXX, XXX−XXX

viscosity, are required to close the solid phase governing equations, which are summarized in Table 1.

$$\frac{\partial(\frac{3}{2}nT_s)}{\partial t} + \nabla\cdot(\frac{3}{2}nT_s\boldsymbol{u}_s) = -(PI + \tau): (\nabla\boldsymbol{u}_s) + \nabla\cdot q - \zeta T_s \quad (7)$$

Table 1. Granular Kinetic Theory Models and Parameters

property	model/parameter
diameter	Sauter-mean
granular viscosity	Gidaspow
granular bulk viscosity	Lun et al.
frictional viscosity	Schaeffer
angle of internal friction	30
solid pressure	Lun et al.
restitution coefficient	0.8

2.2. PBM. To describe the agglomeration and breakage of agglomerates, a particle PBM is used to model the number density of each class of agglomerates.[46−48]

2.2.1. Population Balance Equation (PBE). For particle groups with number density n, velocity $\boldsymbol{u}$, and volume V, the conservation of number density is

$$\frac{\partial}{\partial t}[n(V, t)] + \nabla\cdot[\boldsymbol{u}(V, t)n(V, t)] = B_a(V, t) - D_a(V, t) + B_b(V, t) - D_a(V, t) \quad (8)$$

where the $B_a(V, t)$ and $D_a(V, t)$ terms are due to agglomeration:

$$B_a(V, t) = \frac{1}{2}\int_0^V \alpha(V - V', V')N(V - V', t)N(V', t)\,dV' \quad (9)$$

$$D_a(V, t) = \int_0^\infty \alpha(V, V')N(V, t)N(V', t)dV' \quad (10)$$

where α is the agglomeration kernel, and the $B_b(V, t)$ and $D_b(V, t)$ terms are due to breakage:

$$B_b(V, t) = \int_0^\infty p_0\beta(V')b(V|V')N(V', t)dV' \quad (11)$$

$$D_b(V, t) = \beta(V)N(V) \quad (12)$$

where $\alpha(V-V', V')$ is the agglomeration rate of agglomerates with volume of $V-V'$ and V', p_0 is the number of parent agglomerates broken into subagglomerates, $\beta(V)$ is the probability of fragmentation of agglomerates with volume V, b is the daughter particle distribution function (PDF), $b(V|V')$ is the probability of breaking an agglomerate with volume V' into an agglomerate with volume V, and $b(V|V')$ satisfies:

$$\int_0^{V'} b(V|V')dV = 1 \quad (13)$$

$$p\int_0^{V'} m(V)b(V|V')dV = m(V') \quad (14)$$

2.2.2. Agglomeration and Breakage Kernels. In the continuous theory of cohesive particles proposed by Kellogg et al.,[38,39] the agglomeration and breakage kernels, which are caused by agglomerate collision, are expressed by the collision frequency:[49,50]

$$\alpha_c(V, V') = \psi_a(V, V')\frac{\omega(V, V')}{n(V)n(V')} \quad (15)$$

$$\beta_c(V, V') = \psi_b(V, V')\frac{\omega(V, V')}{n(V)n(V')} \quad (16)$$

where $\omega(V, V')$ is the collision frequency, which is expressed by[50]

$$\omega(V, V') = n(V)n(V')\pi d_{V,V'}^3 g_0\left[\frac{4}{d_{V,V'}}\left(\frac{T_s}{\pi}\frac{m_V\mathrm{dof}_V + m_{V'}\mathrm{dof}_{V'}}{m_V m_{V'}}\right)^{1/2} - \frac{2}{3}(\nabla\cdot\boldsymbol{u}_s)\right] \quad (17)$$

The success factors of agglomeration ($\psi_a(V, V')$) and breakage ($\psi_b(V, V')$) are defined as[39]

$$\psi_a(V, V') = \int_0^{v_{a,V,V',crit}} f(v_n)dv_n = 1 - \exp\left[\frac{-v_{a,V,V',crit}^2}{2T_s\left(\frac{3}{m_V\mathrm{dof}_V} + \frac{3}{m_{V'}\mathrm{dof}_{V'}}\right)}\right] \quad (18)$$

$$\psi_b(V, V') = \int_{v_{a,V,V',crit}}^\infty f(v_n)dv_n = \exp\left[\frac{-v_{b,V,V',crit}^2}{2T_s\left(\frac{3}{m_V\mathrm{dof}_V} + \frac{3}{m_{V'}\mathrm{dof}_{V'}}\right)}\right] \quad (19)$$

where $v_{a,V,V',crit}$ and $v_{b,V,V',crit}$ are the critical velocities of agglomeration and breakage, respectively. Normally, agglomerates will agglomerate when colliding at a low velocity and break when colliding at a high velocity. Thus, when the collision velocity is less than the critical agglomeration velocity, all of the collisions will cause agglomeration. When the collision velocity is greater than the critical breakage velocity, the agglomerate will be broken after the collision. The size of the broken agglomerates is determined by the daughter PDF. In this work, the value of the total degrees of freedom of agglomerates is chosen as 3, that is, dof = 3.

The breakage of agglomerates is caused not only by collision but also by the gas flow. In this article, the breakage rate caused by the gas flow is calculated by the Laakkonen breakage kernel,[51] which is expressed by

$$\beta_t = g(V') = C_1\phi^{1/3}\mathrm{erfc}\left(\sqrt{C_2\frac{\sigma}{\rho_s\phi^{2/3}d^{5/3}} + C_3\frac{\mu}{\sqrt{\rho_s\rho_g}\phi^{2/3}d^{5/3}}}\right) \quad (20)$$

where ϕ is the dissipation rate, d is the diameter of the parent agglomerates, C_1, C_2 and C_3 are constant, and erfc is the Gaussian error function:

$$\mathrm{erfc} = \frac{2}{\pi}\int_x^\infty e^{-\eta^2}d\eta \quad (21)$$

https://doi.org/10.1021/acs.iecr.4c00310
Ind. Eng. Chem. Res. XXXX, XXX, XXX−XXX

The daughter PDF is given by

$$b(V|V') = \frac{30}{V'}\left(\frac{V}{V'}\right)^2\left(1 - \frac{V}{V'}\right)^2 \quad (22)$$

Thus, the combined breakage kernel is given by

$$\beta = \sqrt{\beta_c^2 + \beta_t^2} \quad (23)$$

2.2.3. Determination of Critical Velocity. For a given system, the critical velocity of agglomeration and breakage depends on the particle material conditions. As the agglomerate diameter increases, the agglomerate cohesion decreases, which is indicated as a decrease in the agglomeration success factor and an increase in the fragmentation success factor in the agglomeration and breakage kernels. Based on the study of Fang et al.,[52] in this study, the critical agglomeration velocity of the largest agglomerates with a diameter of a few millimeters is chosen in the order of 1 m/s. The success factors of agglomeration and breakage calculated based on the critical velocities are shown in Figure 2. In future studies, the agglomeration and fragmentation velocities can be determined by experiments or discrete particle simulations of agglomerate collisions. It should be noted that because the critical agglomeration velocity should be different for agglomerates of different sizes, the critical agglomeration velocity of agglomerates is determined based on a critical sticking velocity curve (Supporting Information: Figure S1). In the Results and Discussion section, the values of critical velocity shown in the figure are all the critical velocities of the maximum agglomeration.

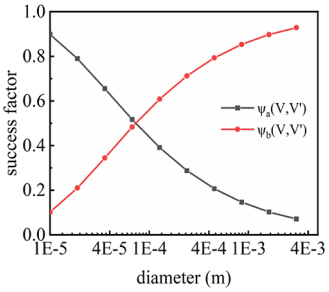

Figure 2. Success factors calculated based on the critical velocities ($v_{a,V,V',crit} = v_{b,V,V',crit}$, $T_s = 1 \times 10^{-5}$ m^2/s^2).

2.3. Simulation and Parameters. A 2D fluidized bed with structured mesh is used as the simulation. The main simulation parameters are given in Table 2. The SiO_2 nanoparticles are used as the bed materials, whose initial agglomerate diameter is chosen as 10 μm, and agglomerate density is 200 kg/m^3 based on the literature.[17,18] The velocity inlet boundary and pressure outlet boundary are used. The wall has a no-slip condition for the gas phase and a partial-slip condition for the solid phase. The time step is chosen as 0.001 s. In the current simulation, the Gidaspow drag models are used, and the restitution coefficient is fixed at 0.8. The effects drag models and restitution coefficient on the volume fraction and size distribution of agglomerate are not sensitive (Supporting Information: Figures S2 and S3).

Table 2. Parameters of a Fluidized Bed System

property	value	units
bed height	0.2	m
bed width	0.02	m
mesh type	quadrilateral mesh	
grid size	1	mm
gas density	1.225	kg/m^3
gas viscosity	1.85×10^{-5}	Pa s
initial particle stacking height	0.1	m
initial particle volume fraction	0.5	

The range of agglomerate diameter is chosen based on experimental results in the literature,[53,54] which ranges from 10 μm to 3 mm and is divided into 10 intervals based on an equal geometric ratio distribution of particle diameter, as listed in Table 3.

Table 3. Average Particle Size of Each Discrete Interval

discrete interval (i)	average particle size (m)
bin-0	0.00304
bin-1	0.00161
bin-2	8.54×10^{-04}
bin-3	4.53×10^{-04}
bin-4	2.4×10^{-04}
bin-5	1.27×10^{-04}
bin-6	6.73×10^{-05}
bin-7	3.56×10^{-05}
bin-8	1.89×10^{-05}
bin-9	1×10^{-05}

The simulations are performed using ANSYS Fluent, with the agglomeration and breakage kernels supplied through user-defined functions. The phase-coupled SIMPLE algorithm is applied for the pressure−velocity coupling. The discrete method is used to solve the PBE.

3. MODEL VALIDATION

3.1. Case 1: Unbounded Riser System. First, the TFM-PBM model is applied to the periodic riser studied by Kellogg et al.[38] to verify the model's accuracy. In their study, the volume fraction of the solid phase is fixed at 0.01. By changing the Hamaker constant to adjust the cohesion strength between particles, the critical velocity of agglomeration $v_{a,V,V',crit}$ is varied from 0.22 to 0.59 cm/s, and the variation curve of the volume fraction of agglomerates at different critical velocities is obtained. The boundary conditions, initial conditions, and other model parameters set by the model are consistent with Kellogg et al. The variation of agglomerate volume fraction with the critical velocity calculated in this article is compared to that of both the DEM model and the continuum model by Kellogg et al.,[38] as shown in Figure 3. It can be seen that the simulation results of the TFM-PBM model in this article are consistent with the continuum model of Kellogg et al.[38]

3.2. Case 2: Fluidized Bed System with Extreme Cases. Second, the model is applied to a fluidized bed with extreme conditions: the only agglomerate condition and the only fragment condition. Figure 4 shows the volume probability distribution of agglomerates in each discrete interval in the fluidized bed at different times. The size distribution and the number density of the agglomerates evolve with time. The rate of fragmentation is lower than the rate of agglomeration. This is because when agglomerates only fragment, the large volume and mass of the agglomerates result in a low collision frequency between the agglomerates. At the condition that the agglomerates only agglomerate, the agglomerates instantly stick together when they collide. The particle size distribution

https://doi.org/10.1021/acs.iecr.4c00310
Ind. Eng. Chem. Res. XXXX, XXX, XXX−XXX

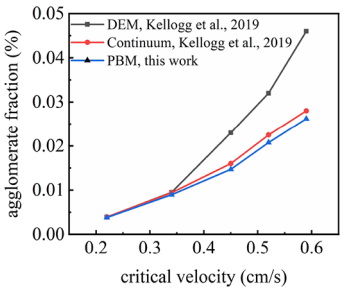

Figure 3. Comparison of the fraction of particles in agglomerates at different critical velocities.

finally reaches a stable state with the largest agglomerates. At the condition that the agglomerates only fragment, the agglomerates break from their maximum diameter, the bed height gradually increases and finally reaches a stable height. The particle size distribution finally reaches a stable state with the smallest agglomerates. According to the comparison of results in these two extreme cases, it can be considered that the model in this article can simulate the fluidization process of agglomerates and obtain the agglomerate distribution in the bed.

3.3. Case 3: Fluidization Behavior Compared with the Experiment. A fluidized bed with an inner diameter of 50 mm and a height of 400 mm is used as the experimental setup. In the simulation, a 2D fluidized bed with a width of 50 mm and height of 400 mm is used. The 20 nm SiO_2 and TiO_2 nanoparticles are used as bed materials, representing different cohesive nanoparticles. The bed height is measured by applying a strong light on the back of the fluidized bed to create a clear contrast between the light and dark areas of the dilute and dense phases so that the bed surface can be clearly observed. In this way, the original particles look black.

According to study,[55,56] the ALD process can be carried out at atmospheric pressure, thus in this study the simulation and experiment are carried out at atmospheric pressure. During the experiment, a differential pressure gauge was used to detect the fluidization pressure in the fluidized bed with an accuracy of 0.1 Pa.

In the simulation, the initial agglomerate diameter is chosen as 10 μm, and the agglomerate density of SiO_2 and TiO_2 nanoparticles is 200 and 650 kg/m^3, respectively. The bed pressure drop, bed expansion ratio, and collapse curve in the fluidized bed of the two kinds of particles are investigated.

Figure 5 shows the simulation and experimental minimal fluidization velocity, bed expansion ratio, and bed collapse curves of SiO_2 nanoparticle agglomerates. The minimal fluidization velocity of the SiO_2 nanoparticles determined by experimental and simulation are similar, which is around 1 cm/s (Figure 5a). From the results, at the beginning, the pressure drop increases linearly with the increase of gas velocity and remains fixed after reaching the minimal fluidization velocity. The four velocities of 1, 2, 3, and 4 cm/s are used for comparison in experiments and simulation studies. For the bed expansion ratio and bed collapse curves at different fluidizing gas velocities, the simulated results are in good agreement with the experimental results.

Figure 6 shows the simulation and experimental results of the TiO_2 nanoparticle agglomerates. The four gas velocities of 5, 6, 7, and 8 cm/s are used for the test. From the simulation results, the minimal fluidization gas velocity of TiO_2 is about 6 cm/s, which is consistent with the experimental result (Figure 6a). Also, the predictions of the bed expansion ratio and the collapse curves generally agree with the experiments. Therefore, the current model is able to predict nanoparticle fluidization at different cohesions.

Comparing the fluidization results of SiO_2 nanoparticles and TiO_2 nanoparticles, it was found that there is a significant difference in their fluidization behavior. This is because the cohesion, density, and other properties of SiO_2 and TiO_2 are different. SiO_2 has a lower cohesion and is prone to fluidization; therefore, the bed expansion ratio increases with the increase of gas velocity. Meanwhile, due to the higher density and cohesion of TiO_2, the bed does not expand significantly at lower gas

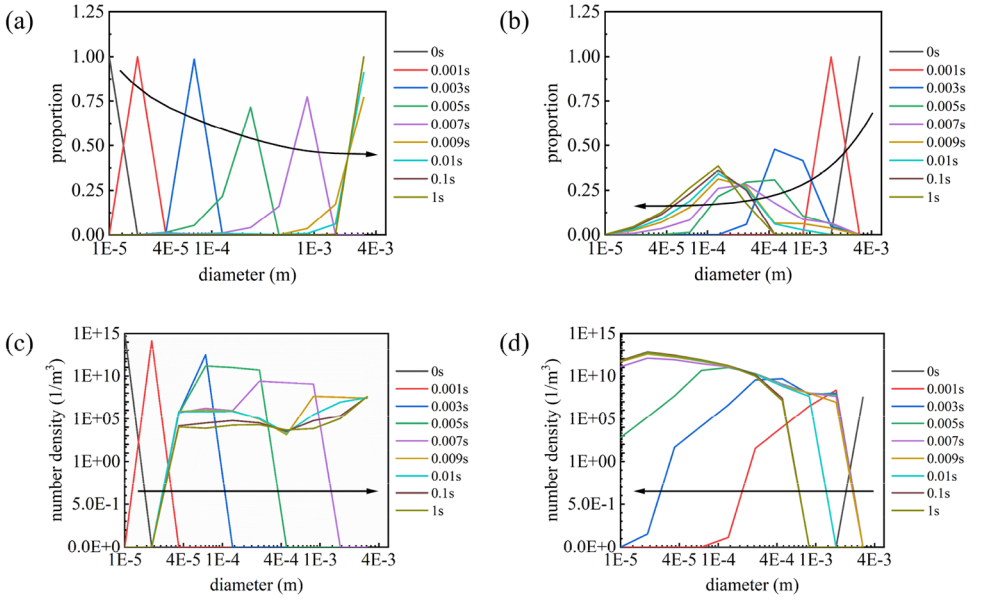

Figure 4. Evolution of volume probability distribution of agglomerates in the fluidized bed: (a) volume probability distribution when the agglomerates only agglomerate; (b) volume probability distribution when the agglomerates only fragment; (c) change of number density over time when the agglomerates only agglomerate; and (d) change of number density over time when the agglomerates only fragment.

https://doi.org/10.1021/acs.iecr.4c00310
Ind. Eng. Chem. Res. XXXX, XXX, XXX−XXX

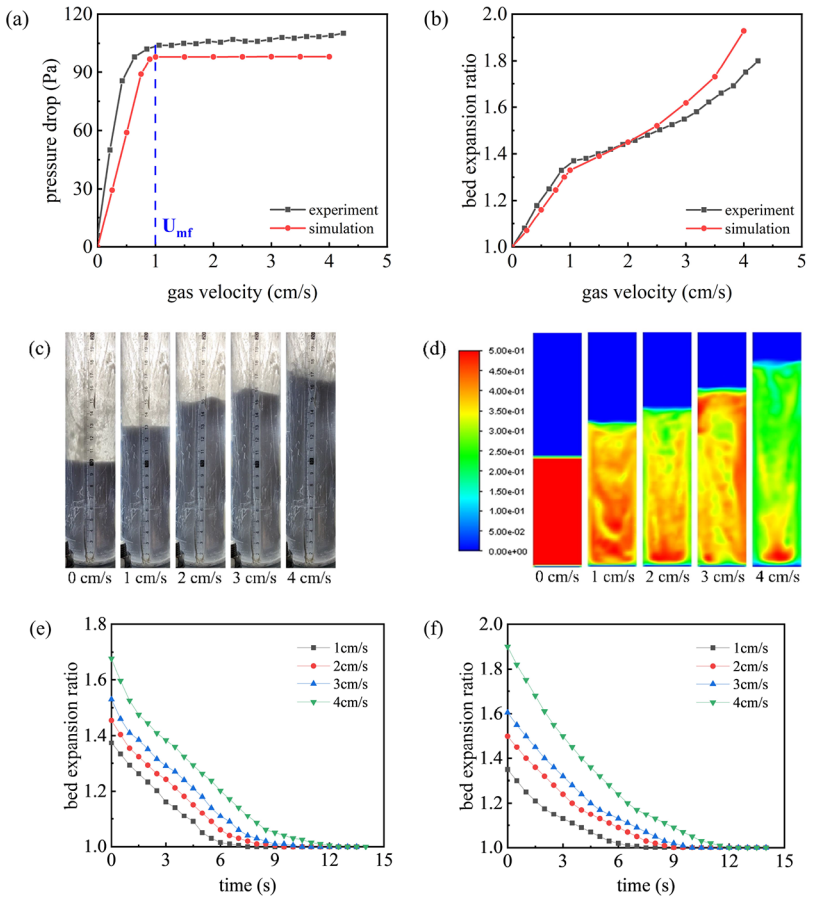

Figure 5. SiO_2 nanoparticle agglomerates: comparison of experimental and simulation results on (a) bed pressure drop and (b) bed expansion ratio; (c) experiment fluidized bed images and (d) simulation fluidized bed images; (e) collapse curve in the simulation results; (f) collapse curve in the simulation results.

velocities. However, when the minimal fluidization velocity is reached, the bed height gradually increases.

4. RESULTS AND DISCUSSION

4.1. Effect of Critical Velocity Ratio. As the cohesion of nanoparticles has a significant influence on fluidization,[25,27,57] the effect of critical agglomeration/breakage velocities is investigated. By keeping the critical agglomeration velocity (v_a) constant at 1 m/s, while varying the critical breakage velocity (v_b) from 0.01 to 10 m/s, the simulations of fluidization at different critical velocity ratios (v_b:v_a) are obtained. As shown in Figure 7, the pressure drop fluctuation with time gradually decreases and finally becomes stable. A significant fluctuation of bed pressure drop is caused by the dynamic formation and fragmentation of agglomerates in gas fluidization.[27] For different conditions, when the time is 15 s, the bed pressure drop is almost stable under different conditions.

Figure 8 shows the variation of volume fraction, volume probability distribution, and diameter of agglomerates for different critical velocity ratios. The bed expansion ratio becomes smaller as the critical velocity ratio increases while keeping the critical agglomeration velocity constant. At the same time, the volume fraction of agglomerates increases and larger agglomerates appear in the bed. The average size of agglomerates increases and the distribution of agglomerates inside the bed becomes more uniform. This is because, at a fixed critical agglomeration velocity, as the critical breakage velocity increases, the relative agglomeration cohesion increases, the agglomerates become more difficult to break, and the bed expansion ratio decreases. At the extreme condition of v_b:v_a = 10:1, an almost static bed with large agglomerates is observed.

Figure 9 shows the variation of PSD distribution over time in the top, middle, and bottom parts of the bed at v_b:v_a = 0.1:1. It can be observed that during the simulation process the average agglomerate size of the top, middle, and bottom parts of the bed first fluctuates and gradually stabilizes with time.

Figures 10−12 show the axial distribution of agglomerate volume fraction, diameter, solid velocity, and gas velocity at different heights. The results at 1/3 and 2/3 of the bed height are taken for comparison. It can be found that, at different bed heights, the solid velocity and gas velocity show profiles similar to "W", which are found to be higher near the bed wall as well as in the middle of the bed. The distributions of the axial gas velocity and agglomerate velocity are similar to the results of Lu et al.[32] For the case of v_b:v_a = 10:1, the movement of agglomerates is very limited, and the gas velocity distribution is uniform in the middle zone of fluidized bed, indicating that the bed behaves like a fixed bed.

Combining Figures 9 and 11, it can be observed that, after stabilization, the volume fraction and diameter of the agglomerates in the lower part of the bed are larger, but the overall distribution of agglomerates within the bed is relatively uniform, which is similar to the experimental results.[53] The agglomerate diameters show a tendency to be larger in the middle and smaller near the bed wall at different bed heights.

https://doi.org/10.1021/acs.iecr.4c00310
Ind. Eng. Chem. Res. XXXX, XXX, XXX−XXX

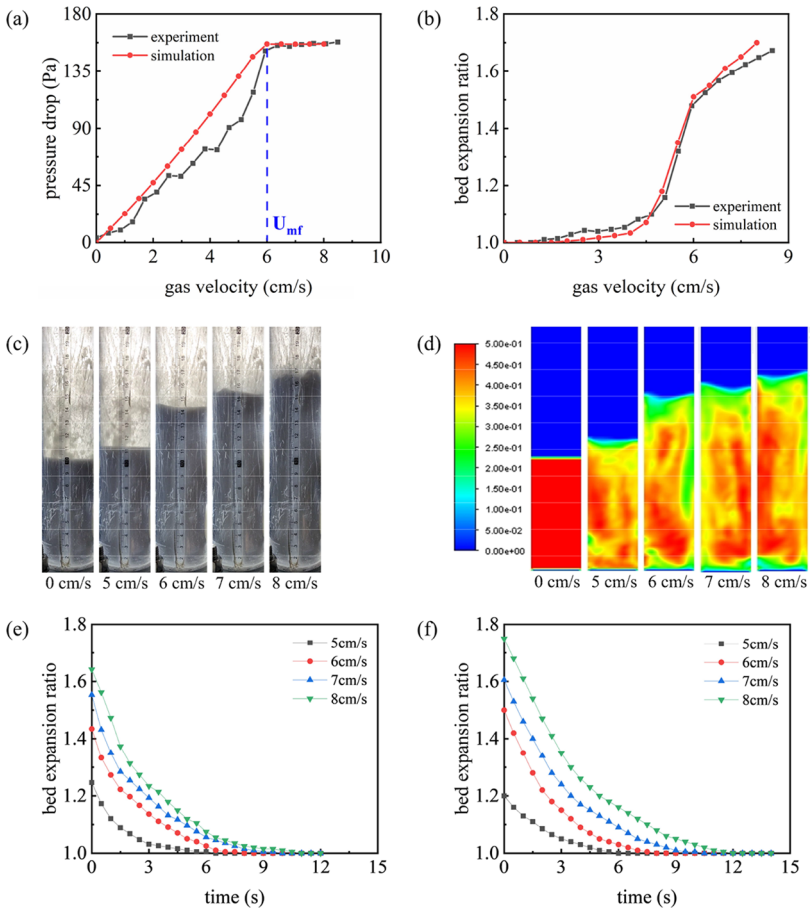

Figure 6. For TiO_2 nanoparticle agglomerates: comparison of experimental and simulation results on (a) bed pressure drop and (b) bed expansion ratio; (c) experimental fluidized bed images and (d) simulation fluidized bed images; (e) collapse curve in the simulation results; (f) collapse curve in the simulation results.

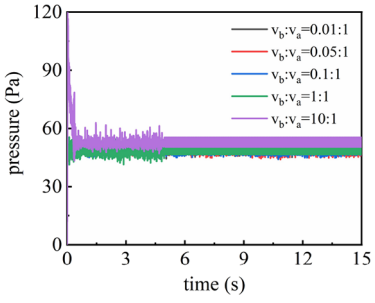

Figure 7. Variation of bed pressure drop with time at different critical velocity ratios.

4.2. Effect of Critical Velocity Values. In this section, the critical velocity ratio is fixed at v_b:v_a = 2:1, which the critical of agglomeration/breakage velocities are changed that are v_b:v_a = 0.2:0.1,0.4:0.2,1:0.5, and 2:1 m/s. Figure 13 shows the variation of volume fraction, the volume probability distribution, and the diameter of agglomerates for different critical velocities. As the critical velocity increases, the bed expansion ratio becomes smaller. At the same time, the volume fraction of agglomerates and the average agglomerate size increase, and the distribution of agglomerates inside the bed becomes more uniform. This is because the agglomerate cohesion increases as the critical velocity increases while maintaining v_b:v_a = 2:1. At this point, the agglomerates are more difficult to break up; thus, the number of large agglomerates increases, and the bed expansion ratio decreases. The gas flow has less influence on the movement of the large agglomerates, resulting in a more uniform distribution of agglomerates within the bed.

4.3. Extension To Predict Fluidization of Fine Particles. Finally, the model is extended to simulate the fluidization of fine particles, which usually show strong cohesion.[58,59] The agglomerate properties and size distribution of fine particles are affected by cohesion, and these properties further affect the fluidization state of fine particles.[60−62] The diameter of the fine particles used in the simulation is 10 μm. The density is 2100 kg/m^3. The fluidizing gas velocity is set to 9 cm/s. The fluidization of fine particles is studied by keeping the critical agglomeration velocity (v_a) constant at 1 m/s, while varying the critical breakage velocity (v_b) from 0.1 to 50 m/s. Figure 14 shows the variation of the bed pressure drop with time for the ratio of fine particles at different critical velocities. With time, large agglomerates continue to form and settle in the fluidized bed, making the bed pressure drop gradually stable. As the critical velocity ratio increases, the bed pressure drop fluctuates.

Figure 15 shows the variation of volume fraction, volume probability distribution, and diameter of agglomerates for different critical velocities for fine particle. A comparison of the results for fine particles with nanoparticle agglomerates shows that the fluidization pattern of fine particles is similar to that of nanoparticle agglomerates. While keeping the critical agglomeration velocity constant, the agglomerates become more cohesive and the bed expansion ratio decreases as the critical

https://doi.org/10.1021/acs.iecr.4c00310
Ind. Eng. Chem. Res. XXXX, XXX, XXX−XXX

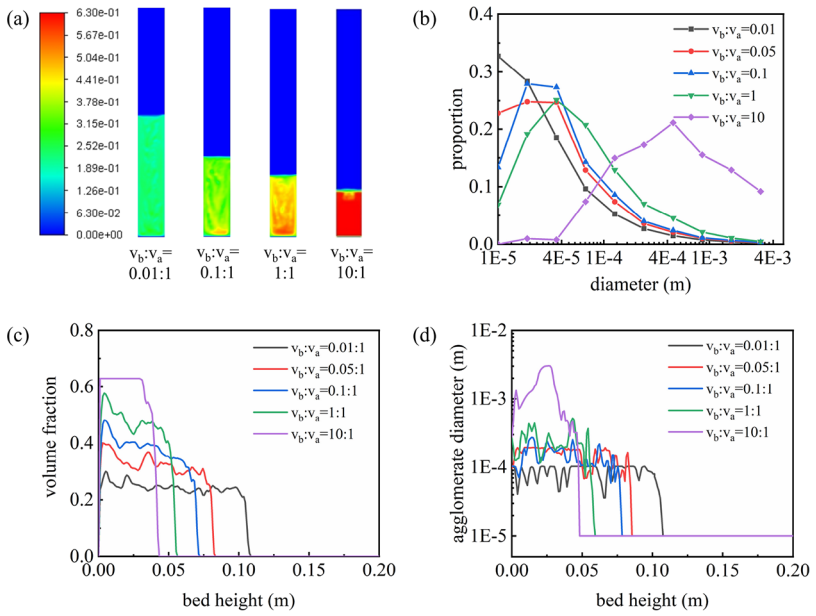

Figure 8. Variation of volume fraction, volume probability distribution, and diameter of agglomerates for different critical velocity ratios at 15 s. (a) Contours of agglomerates volume fraction; (b) volume probability distribution of agglomerate in each discrete interval; (c) distribution of agglomerate volume fraction in the axial direction; (d) distribution of agglomerate diameter in the axial direction.

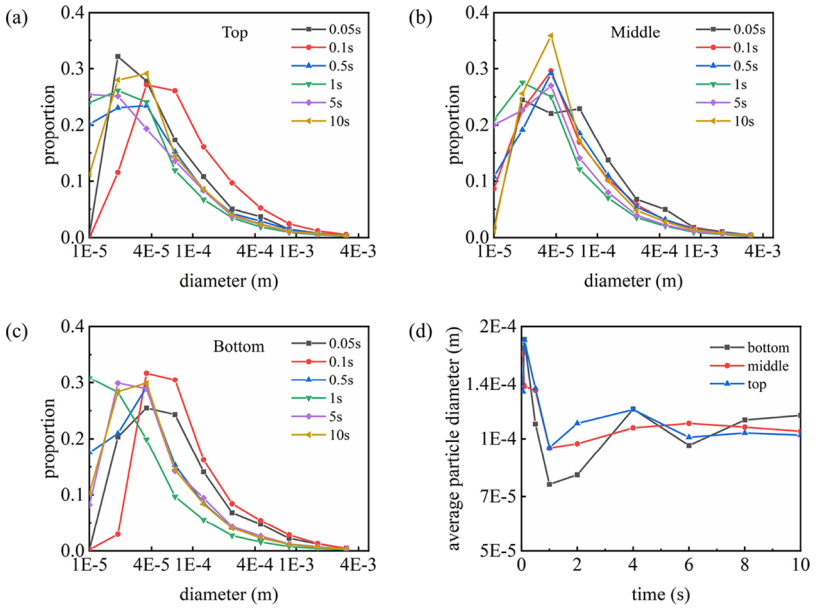

Figure 9. PSD distribution at the (a) top, (b) middle, and (c) bottom of the bed at different times. (d) Variation of average particle size at the top, middle, and bottom of the bed over time.

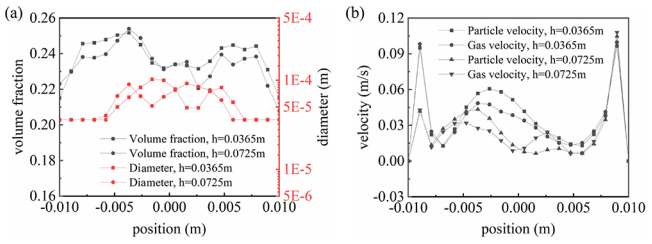

Figure 10. Under condition v_b:v_a = 0.01:1, (a) axial distribution of agglomerate volume fraction and diameter and (b) solid velocity and gas velocity at different heights in the fluidized bed at 15 s.

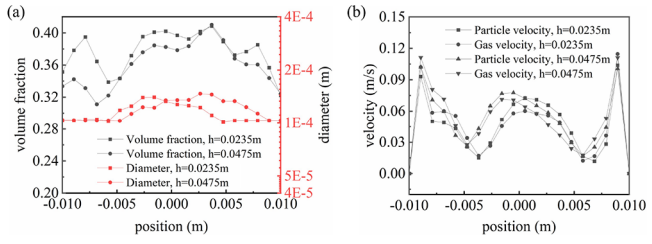

Figure 11. Under condition v_b:v_a = 0.1:1, (a) axial distribution of agglomerate volume fraction and diameter and (b) solid velocity and gas velocity at different heights in the fluidized bed at 15 s.

https://doi.org/10.1021/acs.iecr.4c00310
Ind. Eng. Chem. Res. XXXX, XXX, XXX−XXX

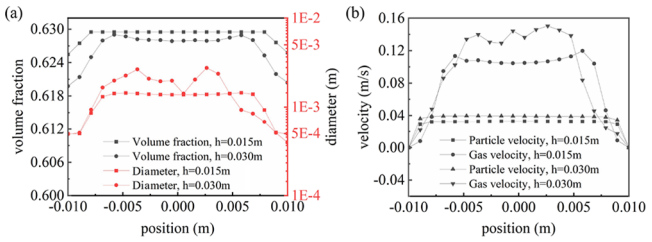

Figure 12. Under condition v_b:v_a = 10:1, (a) axial distribution of agglomerate volume fraction and diameter and (b) solid velocity and gas velocity at different heights in the fluidized bed at 15 s.

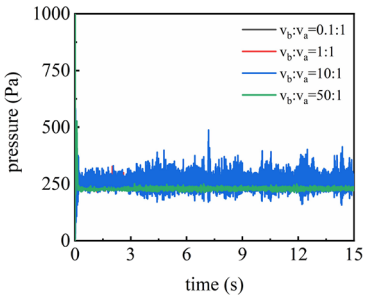

Figure 14. Variation of bed pressure drop with time at different critical velocity ratios.

breakage velocity increases. At the same time, the volume fraction of agglomerates and the proportion of large agglomerates increase, and the distribution of agglomerates becomes more uniform.

The comparison also shows that the volume distribution of the fine particles is less homogeneous compared to that of nanoparticle agglomerates at the same critical velocity conditions. This is due to the fact that fine particles with a higher density promote a bubbling fluidization state, which is consistent with the fluidization of fine particles.[59] The presence of bubbles in the fluidized bed would increase the inhomogeneity of the volume fraction distribution of the agglomerates in the bed.

5. CONCLUSIONS

1. The continuum theory of Kellogg et al.[39] is combined with a general PBM model and applied to a gas−solid nanoparticle agglomerate fluidized bed with a high cohesion and wide agglomerate size distribution. The ratio of critical breakage velocity to critical agglomeration velocity is used to characterize the cohesion of nanoparticles.
2. The model is validated with two cases: an unbounded riser system and extreme conditions in a fluidized bed. In the riser system, the predictions of the agglomerate fraction are consistent with the continuum model. In the fluidized bed, the TFM-PBM model can well predict the probability distribution of agglomerates under only agglomeration or only breakage conditions.
3. The fluidization properties of SiO_2 and TiO_2 nanoparticles are predicted and compared with experiments. There is good consistency in the simulations and experiments for the bed pressure drop, fluidization, and bed collapse curves. The TFM-PBM model can effectively predict the basic characteristics of fluidized nanoparticle agglomerates.
4. In the model, keeping the critical agglomeration velocity constant, as the ratio of critical breakage velocity increases, the bed expansion ratio decreases, the average agglomerate size increases, and the volume fraction and diameter of the agglomerates in the lower part of the bed become larger. Fixing $v_{a,\,crit}$: $v_{b,\,crit}$ = 1:2, as the critical velocity increases, the bed expansion ratio decreases and the average agglomerate size increases.
5. The ability to simulate the fluidization of fine particles is also checked. At the same critical velocity conditions, a more inhomogeneous distribution of fine particles is

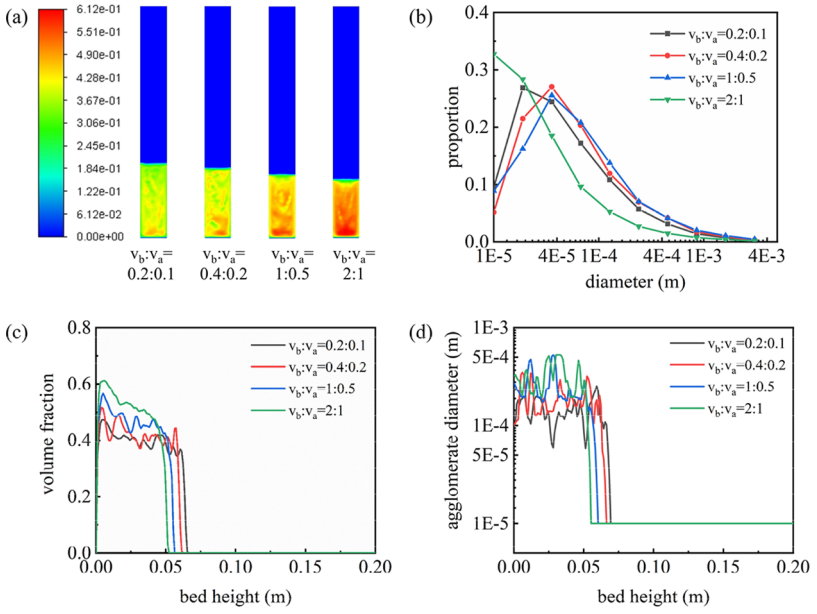

Figure 13. Variation of volume fraction, volume probability distribution, and diameter of agglomerates for different critical velocity at 15 s. (a) Contours of agglomerate volume fraction; (b) volume probability distribution of agglomerate in each discrete interval; (c) distribution of agglomerate volume fraction in the axial direction; (d) distribution of agglomerate diameter in the axial direction.

https://doi.org/10.1021/acs.iecr.4c00310
Ind. Eng. Chem. Res. XXXX, XXX, XXX−XXX

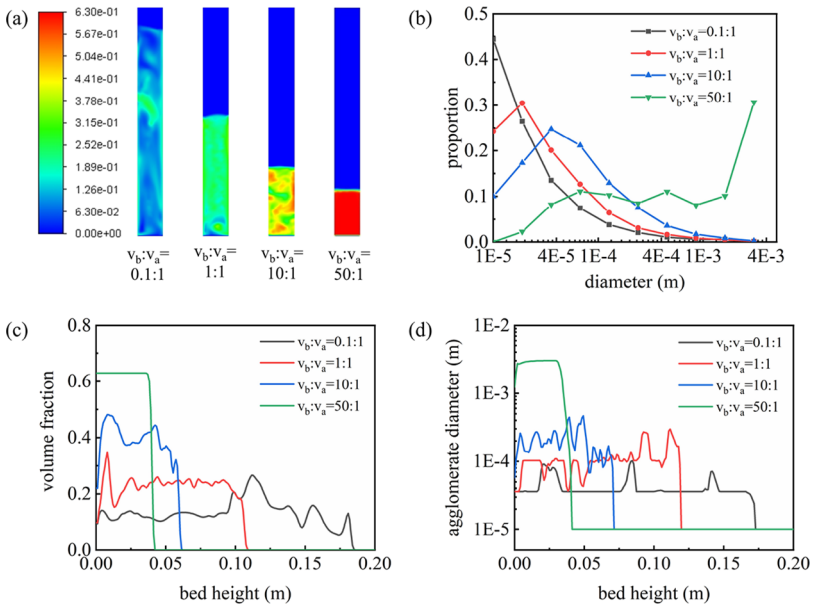

Figure 15. Variation of volume fraction, volume probability distribution, and diameter of agglomerates for different critical velocity ratio for fine particles at 15 s: (a) contours of agglomerate volume fraction; (b) volume probability distribution of agglomerate in each discrete interval; (c) distribution of agglomerate volume fraction in the axial direction; (d) distribution of agglomerate diameter in the axial direction.

observed compared to that of the nanoparticle agglomerates.

■ ASSOCIATED CONTENT

Supporting Information

The Supporting Information is available free of charge at https://pubs.acs.org/doi/10.1021/acs.iecr.4c00310.

Plot of the critical sticking velocity with the agglomerate diameter; distribution of agglomerate volume fraction in the axial direction and the volume probability distribution of agglomerate under different drag models; and distribution of agglomerate volume fraction in the axial direction and the volume probability distribution of agglomerate under different restitution coefficients (PDF)

■ AUTHOR INFORMATION

Corresponding Author

Daoyin Liu − *Key Laboratory of Energy Thermal Conversion and Control of Ministry of Education, School of Energy and Environment, Southeast University, 210096 Nanjing, Jiangsu, China;* orcid.org/0000-0003-1746-2204; Email: dyliu@seu.edu.cn

Authors

Yan Wu − *Key Laboratory of Energy Thermal Conversion and Control of Ministry of Education, School of Energy and Environment, Southeast University, 210096 Nanjing, Jiangsu, China*

Berend G. M. van Wachem − *Lehrstuhl für Mechanische Verfahrenstechnik, Fakultät für Verfahrens- und Systemtechnik, Otto-von-Guericke-Universität Magdeburg, D-39106 Magdeburg, Germany*

J. Ruud van Ommen − *Department of Chemical Engineering, Delft University of Technology, 2629 HZ Delft, The Netherlands;* orcid.org/0000-0001-7884-0323

Complete contact information is available at: https://pubs.acs.org/10.1021/acs.iecr.4c00310

Notes

The authors declare no competing financial interest.

■ ACKNOWLEDGMENTS

Financial support by the National Natural Science Foundation of China (Nos. 52376141 and 51676042) is gratefully acknowledged.

■ REFERENCES

(1) George, S. M. Atomic Layer Deposition: An Overview. *Chem. Rev.* **2010**, *110* (1), 111−131.

(2) Puurunen, R. L. Surface chemistry of atomic layer deposition: A case study for the trimethylaluminum/water process. *J. Appl. Phys.* **2005**, *97*, 121301−121352.

(3) Hu, Y.; Lu, J.; Feng, H. Surface modification and functionalization of powder materials by atomic layer deposition: a review. *RSC Adv.* **2021**, *11* (20), 11918−11942.

(4) Li, Z.; Li, J.; Liu, X.; Chen, R. Progress in enhanced fluidization process for particle coating via atomic layer deposition. *Chem. Eng. Process.* **2021**, *159*, No. 108234.

(5) van Ommen, J. R.; Yurteri, C. U.; Ellis, N.; Kelder, E. M. Scalable gas-phase processes to create nanostructured particles. *Particuology* **2010**, *8* (6), 572−577.

(6) Liang, X.; Zhou, Y.; Li, J.; Weimer, A. W. Reaction mechanism studies for platinum nanoparticle growth by atomic layer deposition. *J. Nanopart. Res.* **2011**, *13* (9), 3781−3788.

(7) Li, J.; Liang, X.; King, D. M.; Jiang, Y.-B.; Weimer, A. W. Highly dispersed Pt nanoparticle catalyst prepared by atomic layer deposition. *Appl. Catal., B* **2010**, *97* (1), 220−226.

(8) Faqih, A.; Chaudhuri, B.; Muzzio, F. J.; Tomassone, M. S.; Alexander, A.; Hammond, S. Flow - induced dilation of cohesive granular materials. *AlChE J.* **2006**, *52* (12), 4124−4132.

(9) Wang, J.; Xu, B.; Zhou, T.; Liang, X. Agglomeration Mechanism of Nanoparticles by Adding Coarse Fluid Catalytic Cracking Particles. *Chem. Eng. Technol.* **2016**, *39* (8), 1490−1496.

(10) Bahramian, A. The mutual effects between the interparticle forces and mechanical properties on fluidization of TiO_2 nanoparticle

agglomerates in a conical fluidized bed: nanoindentation and pressure fluctuation analysis. *J. Nanopart. Res.* **2019**, *21* (9), 196.
(11) Yin, L.; Zhong, Z.. Nanoparticles. In *Biomaterials Science* (4th ed.); Wagner, W. R.; Sakiyama-Elbert, S. E.; Zhang, G.; Yaszemski, M. J. Eds.; Academic Press; 2020; pp 453−483.
(12) Rizwan, M.; Shoukat, A.; Ayub, A.; Razzaq, B.; Tahir, M. B. Chapter 3 - Types and classification of nanomaterials. In *Nanomaterials: Synthesis, Characterization, Hazards and Safety*; Tahir, M. B.; Sagir, M.; Asiri, A. M. Eds.; Elsevier: 2021; pp 31−54.
(13) Zhu, C.; Yu, Q.; Dave, R. N.; Pfeffer, R. Gas fluidization characteristics of nanoparticle agglomerates. *AlChE J.* **2005**, *51* (2), 426−439.
(14) Hakim, L. F.; Portman, J. L.; Casper, M. D.; Weimer, A. W. Aggregation behavior of nanoparticles in fluidized beds. *Powder Technol.* **2005**, *160* (3), 149−160.
(15) van Ommen, J. R.; Valverde, J. M.; Pfeffer, R. Fluidization of nanopowders: a review. *J. Nanopart. Res.* **2012**, *14* (3), 737.
(16) Wang, X. S.; Palero, V.; Soria, J.; Rhodes, M. J. Laser-based planar imaging of nano-particle fluidization: Part II—mechanistic analysis of nanoparticle aggregation. *Chem. Eng. Sci.* **2006**, *61* (24), 8040−8049.
(17) de Martín, L.; Bouwman, W. G.; van Ommen, J. R. Multidimensional Nature of Fluidized Nanoparticle Agglomerates. *Langmuir* **2014**, *30* (42), 12696−12702.
(18) Valverde, J. M.; Castellanos, A. Fluidization, bubbling and jamming of nanoparticle agglomerates. *Chem. Eng. Sci.* **2007**, *62* (23), 6947−6956.
(19) Knemeyer, K.; Baumgarten, R.; Ingale, P.; Naumann d'Alnoncourt, R.; Driess, M.; Rosowski, F. Toolbox for atomic layer deposition process development on high surface area powders. *Rev. Sci. Instrum.* **2021**, *92* (2), No. 025115.
(20) Richey, N. E.; de Paula, C.; Bent, S. F. Understanding chemical and physical mechanisms in atomic layer deposition. *J. Chem. Phys.* **2020**, *152* (4), No. 040902.
(21) LaMarche, W. C. Q.; Liu, P.; Kellogg, K. M.; Lattanzi, A. M.; Hrenya, C. M. Toward general regime maps for cohesive-particle flows: Force versus energy-based descriptions and relevant dimensionless groups. *AlChE J.* **2021**, *67* (9), No. e17337.
(22) Liu, D.; van Wachem, B. G. M.; Mudde, R. F.; Chen, X.; van Ommen, J. R. An adhesive CFD-DEM model for simulating nanoparticle agglomerate fluidization. *AlChE J.* **2016**, *62* (7), 2259−2270.
(23) Ye, M.; van der Hoef, M. A.; Kuipers, J. A. M. A numerical study of fluidization behavior of Geldart A particles using a discrete particle model. *Powder Technol.* **2004**, *139* (2), 129−139.
(24) Cundall, P. A.; Strack, O. D. L. A discrete numerical model for granular assemblies. *Géotechnique* **1979**, *29* (1), 47−65.
(25) Seville, J. P. K.; Willett, C. D.; Knight, P. C. Interparticle forces in fluidisation: a review. *Powder Technol.* **2000**, *113* (3), 261−268.
(26) Li, T.; Rabha, S.; Verma, V.; Dietiker, J.-F.; Xu, Y.; Lu, L.; Rogers, W.; Gopalan, B.; Breault, G.; Tucker, J.; Panday, R. Experimental study and discrete element method simulation of Geldart Group A particles in a small-scale fluidized bed. *Adv. Powder Technol.* **2017**, *28* (11), 2961−2973.
(27) Wu, Y.; Hou, Q.; Yu, A. Linking discrete particle simulation to continuum properties of the gas fluidization of cohesive particles. *AlChE J.* **2020**, *66* (5), No. e16944.
(28) Bahramian, A.; Olazar, M. Particle Adhesion Effects on Particle Size Distribution of Titania Nanoparticle Agglomerates in a Conical Fluidized Bed: A Computational Fluid Dynamics and Discrete Element Method Adhesive Approach. *Ind. Eng. Chem. Res.* **2023**, *62* (50), 21835−21851.
(29) Fullmer, W. D.; Hrenya, C. M. The Clustering Instability in Rapid Granular and Gas-Solid Flows. *Annu. Rev. Fluid Mech.* **2017**, *49* (1), 485−510.
(30) Motlagh, A. H. A.; Grace, J. R.; Salcudean, M.; Hrenya, C. M. New structure-based model for Eulerian simulation of hydrodynamics in gas−solid fluidized beds of Geldart group "A" particles. *Chem. Eng. Sci.* **2014**, *120*, 22−36.
(31) van Wachem, B.; Sasic, S. Derivation, simulation and validation of a cohesive particle flow CFD model. *AlChE J.* **2008**, *54* (1), 9−19.
(32) Lu, H.; Wang, S.; Zheng, J.; Gidaspow, D.; Ding, J.; Li, X. Numerical simulation of flow behavior of agglomerates in gas−cohesive particles fluidized beds using agglomerates-based approach. *Chem. Eng. Sci.* **2010**, *65* (4), 1462−1473.
(33) Askarishahi, M.; Salehi, M. S.; Radl, S. Capability of the TFM Approach to Predict Fluidization of Cohesive Powders. *Ind. Eng. Chem. Res.* **2022**, *61* (8), 3186−3205.
(34) Wei, L.; Gu, Y.; Wang, Y.; Lu, Y. Multi-fluid Eulerian simulation of fluidization characteristics of mildly-cohesive particles: Cohesive parameter determination and granular flow kinetic model evaluation. *Powder Technol.* **2020**, *364*, 264−275.
(35) Niu, L.; Chu, Z.; Cai, M.; Liu, M. Modified Force Balance Model of Estimating Agglomerate Sizes in a Gas−Solid Fluidized Bed. *Ind. Eng. Chem. Res.* **2019**, *58* (19), 8472−8483.
(36) Li, Q.; Yuan, X.; Zhang, M.; Xu, W.; Huo, L.; Mu, Q. A modified agglomeration kernel model used for particle agglomeration. *Adv. Powder Technol.* **2022**, *33* (1), 103349.
(37) Chen, S.; Li, S.; Marshall, J. S. Exponential scaling in early-stage agglomeration of adhesive particles in turbulence. *Phys. Rev. Fluids* **2019**, *4* (2), No. 024304.
(38) Kellogg, K. M.; Liu, P.; Hrenya, C. M. Continuum prediction of entrainment rates and agglomeration of gas-fluidized, lightly-cohesive particles. *Chem. Eng. Sci.* **2019**, *199*, 249−257.
(39) Kellogg, K. M.; Liu, P.; LaMarche, C. Q.; Hrenya, C. M. Continuum theory for rapid cohesive-particle flows: general balance equations and discrete-element-method-based closure of cohesion-specific quantities. *J. Fluid Mech.* **2017**, *832*, 345−382.
(40) Bhoi, S.; Kolan, S. R.; Bück, A.; Tsotsas, E. Population balance modeling of formation and breakage of nanoparticle agglomerates in a spouted bed. *Powder Technol.* **2024**, *433*, No. 119271.
(41) Ding, J.; Gidaspow, D. A bubbling fluidization model using kinetic theory of granular flow. *AlChE J.* **1990**, *36* (4), 523−538.
(42) Patil, D. J.; van Sint Annaland, M.; Kuipers, J. A. M. Critical comparison of hydrodynamic models for gas-solid fluidized beds - Part I: bubbling gas-solid fludized beds operated with a jet. *Chem. Eng. Sci.* **2005**, *60* (1), 57−72.
(43) Taghipour, F.; Ellis, N.; Wong, C. Experimental and computational study of gas−solid fluidized bed hydrodynamics. *Chem. Eng. Sci.* **2005**, *60* (24), 6857−6867.
(44) van Wachem, B. G. M.; Schouten, J. C.; van den Bleek, C. M.; Krishna, R.; Sinclair, J. L. Comparative analysis of CFD models of dense gas−solid systems. *AlChE J.* **2001**, *47* (5), 1035−1051.
(45) Van Wachem, B.. Eulerian−Eulerian modeling approach for turbulent particle-laden flows. In *Modeling Approaches and Computational Methods for Particle-Laden Turbulent Flows*; Subramaniam, S.; Balachandar, S. Eds.; Academic Press: 2023; pp 449−481.
(46) Ramkrishna, D. *Population balances: Theory and applications to particulate systems in engineering*; Elsevier: San Diego, 2000.
(47) Shiea, M.; Buffo, A.; Vanni, M.; Marchisio, D. Numerical Methods for the Solution of Population Balance Equations Coupled with Computational Fluid Dynamics. *Annu. Rev. Chem. Biomol. Eng.* **2020**, *11* (1), 339−366.
(48) O'Sullivan, D.; Rigopoulos, S. A conservative finite volume method for the population balance equation with aggregation, fragmentation, nucleation and growth. *Chem. Eng. Sci.* **2022**, *263*, No. 117925.
(49) Fan, R.; Marchisio, D. L.; Fox, R. O. Application of the direct quadrature method of moments to polydisperse gas−solid fluidized beds. *Powder Technol.* **2004**, *139* (1), 7−20.
(50) Goldschmidt, M. J. V. *Hydrodynamic Modelling of Fluidised Bed Spray Granulation*; Twente University Press (TUP): Enschede, 2001.
(51) Laakkonen, M.; Alopaeus, V.; Aittamaa, J. Validation of bubble breakage, coalescence and mass transfer models for gas−liquid dispersion in agitated vessel. *Chem. Eng. Sci.* **2006**, *61* (1), 218−228.
(52) Fang, Z.; Zhang, Y.; Wei, M.; Zhao, S.; Sun, L.; Wu, X. The critical sticking velocity of non-spherical graphite particles: A numerical study and validation. *Nucl. Eng. Des.* **2020**, *359*, No. 110453.

https://doi.org/10.1021/acs.iecr.4c00310
Ind. Eng. Chem. Res. XXXX, XXX, XXX−XXX

(53) Zhao, Z.; Liu, D.; Ma, J.; Chen, X. Fluidization of nanoparticle agglomerates assisted by combining vibration and stirring methods. *Chem. Eng. J.* **2020**, *388*, No. 124213.
(54) Feng, Z.; Liu, D.; Zhang, W.; Feng, H.; Ruud Van Ommen, J. Elutriation and agglomerate size distribution in a silica nanoparticle vibro-fluidized bed. *Chem. Eng. J.* **2022**, *434*, No. 134654.
(55) Beetstra, R.; Lafont, U.; Nijenhuis, J.; Kelder, E. M.; van Ommen, J. R. Atmospheric Pressure Process for Coating Particles Using Atomic Layer Deposition. *Chem. Vap. Deposition* **2009**, *15* (7−9), 227−233.
(56) Valdesueiro, D.; Meesters, G. M. H.; Kreutzer, M. T.; van Ommen, J. R. Gas-Phase Deposition of Ultrathin Aluminium Oxide Films on Nanoparticles at Ambient Conditions. *Materials* **2015**, *8* (3), 1249−1263.
(57) Galvin, J. E.; Benyahia, S. The effect of cohesive forces on the fluidization of aeratable powders. *AlChE J.* **2014**, *60* (2), 473−484.
(58) Xie, H. Y. The role of interparticle forces in the fluidization of fine particles. *Powder Technol.* **1997**, *94* (2), 99−108.
(59) Wang, Z.; Kwauk, M.; Li, H. Fluidization of fine particles. *Chem. Eng. Sci.* **1998**, *53* (3), 377−395.
(60) Valverde, J. M.; Quintanilla, M. A. S.; Castellanos, A.; Lepek, D.; Quevedo, J.; Dave, R. N.; Pfeffer, R. Fluidization of fine and ultrafine particles using nitrogen and neon as fluidizing gases. *AlChE J.* **2008**, *54* (1), 86−103.
(61) Gan, J.; Zhou, Z.; Yu, A. CFD−DEM modeling of gas fluidization of fine ellipsoidal particles. *AlChE J.* **2016**, *62* (1), 62−77.
(62) Raganati, F.; Chirone, R.; Ammendola, P. Gas−solid fluidization of cohesive powders. *Chem. Eng. Res. Des.* **2018**, *133*, 347−387.

https://doi.org/10.1021/acs.iecr.4c00310
Ind. Eng. Chem. Res. XXXX, XXX, XXX−XXX